

Effects of vacancy and external electric field on the electronic properties of the $MoSi_2N_4$/graphene heterostructure

Qian Liang(梁前), Xiangyan Luo(罗祥燕), Guolin Qian(钱国林), Yuanfan Wang(王远帆), Yongchao Liang(梁永超), and Quan Xie(谢泉)

Citation: Chin. Phys. B, 2024, 33 (**3**): 037101. DOI: 10.1088/1674-1056/acef04
Journal homepage: http://cpb.iphy.ac.cn; http://iopscience.iop.org/cpb

What follows is a list of articles you may be interested in

Blue phosphorene/$MoSi_2N_4$ van der Waals type-II heterostructure: Highly efficient bifunctional materials for photocatalytics and photovoltaics

Xiaohua Li(李晓华), Baoji Wang(王宝基), and Sanhuang Ke(柯三黄)
Chin. Phys. B, 2023, 32 (**2**): 027104. DOI: 10.1088/1674-1056/ac9469

Modulation of Schottky barrier in XSi_2N_4/graphene (X=Mo and W) heterojunctions by biaxial strain

Qian Liang(梁前), Xiang-Yan Luo(罗祥燕), Yi-Xin Wang(王熠欣), Yong-Chao Liang(梁永超), and Quan Xie(谢泉)
Chin. Phys. B, 2022, 31 (**8**): 087101. DOI: 10.1088/1674-1056/ac5c3b

Electronic and optical properties of 3N-doped graphdiyne/MoS_2 heterostructures tuned by biaxial strain and external electric field

Dong Wei(魏东), Yi Li(李依), Zhen Feng(冯振), Gaofu Guo(郭高甫), Yaqiang Ma(马亚强), Heng Yu(余恒), Qingqing Luo(骆晴晴), Yanan Tang(唐亚楠), and Xianqi Dai(戴宪起)
Chin. Phys. B, 2021, 30 (**11**): 117103. DOI: 10.1088/1674-1056/ac1927

Tuning transport coefficients of monolayer $MoSi_2N_4$ with biaxial strain

Xiao-Shu Guo(郭小姝) and San-Dong Guo(郭三栋)
Chin. Phys. B, 2021, 30 (**6**): 067102. DOI: 10.1088/1674-1056/abdb22

Ab initio calculations on oxygen vacancy defects in strained amorphous silica

Bao-Hua Zhou(周保花), Fu-Jie Zhang(张福杰), Xiao Liu(刘笑), Yu Song(宋宇), Xu Zuo(左旭)
Chin. Phys. B, 2020, 29 (**4**): 047103. DOI: 10.1088/1674-1056/ab75db

---

Effects of vacancy and external electric field on the electronic properties of the $MoSi_2N_4$/graphene heterostructure

Qian Liang(梁前), Xiangyan Luo(罗祥燕), Guolin Qian(钱国林),
Yuanfan Wang(王远帆), Yongchao Liang(梁永超), and Quan Xie(谢泉)†

College of Big Data and Information Engineering, Institute of New Optoelectronic Materials and Technology, Guizhou University, Guiyang 550025, *China*

(Received 5 May 2023; revised manuscript received 3 August 2023; accepted manuscript online 11 August 2023)

Recently, the newly synthesized septuple-atomic layer two-dimensional (2D) material $MoSi_2N_4$ (MSN) has attracted attention worldwide. Our work delves into the effect of vacancies and external electric fields on the electronic properties of the MSN/graphene (Gr) heterostructure using first-principles calculation. We find that four types of defective structures, N-in, N-out, Si and Mo vacancy defects of monolayer MSN and MSN/Gr heterostructure are stable in air. Moreover, vacancy defects can effectively modulate the charge transfer at the interface of the MSN/Gr heterostructure as well as the work function of the pristine monolayer MSN and MSN/Gr heterostructure. Finally, the application of an external electric field enables the dynamic switching between n-type and p-type Schottky contacts. Our work may offer the possibility of exceeding the capabilities of conventional Schottky diodes based on MSN/Gr heterostructures.

Keywords: $MoSi_2N_4$, vacancy defects, external electric field, Schottky contacts

PACS: 71.20.–b, 73.30.+y, 61.72.–y **DOI:** 10.1088/1674-1056/acef04

1. Introduction

In recent years, 2D materials have received much scientific attention due to their novel electronic transport, piezoelectric, optical and mechanical properties.[1–5] Among all 2D materials, graphene (Gr),[6,7] hexagonal boron nitride (h-BN),[8–10] phosphorene,[11,12] arsenene[13,14] and transition-metal dichalcogenides (TMDs)[15–17] are the most important and widely researched. MoS_2[18,19] is a typical representative of TMDs, which is extensively used as a channel material in transistors with promising application prospects. In particular, MoS_2 has great potential for applications in photocatalysis,[20] Li-ion batteries,[21] field-effect transistors (FETs),[22] energy storage,[23] sensors,[24] etc. Subsequently, the emergence of 2D van der Waals (vdW) heterostructures stacked by two 2D materials has surprised researchers with some unanticipated results. For instance, Zhang *et al.*[25] proved that MoS_2/g-C_3N_4 heterojunction enhances the hole separation and transfer ability of photogenerated electrons by broadening the spectral absorption range, showing excellent photocatalytic performance. Huang *et al.*[26] successfully synthesized a MoS_2/Gr heterostructure using the facile hydrothermal method, and they found that the MoS_2/Gr heterostructure exhibits preferable photo-response activity under the irradiation of sunlight. Mikhaleva *et al.*[27] reported that the combination of VS_2 monolayer with Gr has good lithium capacity, remarkable electronic conductance and high sorption/desorption rates, making it a promising anode material for Li-ion batteries. Neupane *et al.*[28,29] investigated the Gr/MoS_2 heterostructure systematically using first-principles calculation. They found that non-magnetic Gr/MoS_2 heterostructure changes to magnetic material as a result of Mo site vacancy defects. Furthermore, the C vacancy defect also makes the original non-magnetic water-adsorbed Gr/MoS_2 heterostructure into a magnetic system and the spins of electrons in 2s and 2p orbitals of C atoms give the principal effect of magnetism in water-adsorbed Gr/MoS_2 heterostructure materials with C sites vacancy defects.

More recently, two new layered 2D materials, $MoSi_2N_4$ (MSN) and WSi_2N_4 (WSN), were successfully synthesized by Hong *et al.*,[30] who used the chemical vapor deposition (CVD) method. They also predicted an emerging MA_2Z_4 family by first-principles calculation, where M is a transition metal (Mo, W, V, Nb, Ta, Ti, Zr, Hf or Cr), A is Si or Ge, and Z denotes N, P or As. Lu *et al.*[31] found that 2D MSN modified with 3d transition-metal (TM) atoms can be an effective alternative to noble metal-based catalysts for energy conversion and storage. By constructing a novel Janus MoSH/MSN heterostructure, Nguyen *et al.*[32] found that vertical strain and electric field can achieve n–p type Schottky contact transitions and even ohmic contacts. Xiao *et al.*[33] systematically investigated the catalytic activity of TM atoms and non-metal atom-doped MSN monolayer for hydrogen evolution reaction (HER), and they found that the O, P, Fe and Nb atom-doped systems can be selected as promising HER electrocatalysts with relatively good structural stability.

The electronic properties of 2D vdW heterostructures are sensitive to doping, adsorption, vacancy defect, biaxial strain and external electric field. In this contribution, we construct an

†Corresponding author. E-mail: qxie@gzu.edu.cn

© 2024 Chinese Physical Society and IOP Publishing Ltd

MSN/Gr heterostructure and investigate the effects of vacancy and external electric field on the electronic properties of the MSN/Gr heterostructure based on density functional theory (DFT). First, we compare the band structure of the MSN/Gr heterostructure with the band structures of MSN and Gr, and find that it is a simple superposition of two monolayers. The calculated binding energy is −0.69 eV, and the negative binding energy proves that the MSN/Gr heterostructure we have built is stable. Then, we investigate the effect of vacancy defects on the magnetic properties, work function, charge transfer at the interface and electrostatic potential of MSN monolayer or MSN/Gr heterostructure, respectively. Finally, we study the modulation effect of the external electric field on the MSN/Gr heterostructure.

2. Method

First-principles calculations were performed to obtain the electronic properties of the intrinsic MSN/Gr heterostructure and its defective structures using the Vienna *ab initio* simulation package (VASP)[34,35] based on DFT. The exchange–correlation potential between the interacted electrons was described by the generalized gradient approximation (GGA) with the Perdew–Burke–Ernzerhof (PBE)[36] functional. The projected augmented wave (PAW) potential[37] was used to describe the interactions between ionic cores and valence electrons. The plane-wave kinetic cutoff energy was set to be 500 eV and the reciprocal space was sampled with a $9\times9\times1$ Monkhorst–Pack mesh grid. The convergence criteria for energy and force were set to be 1×10^{-6} eV and 0.01 eV/Å, respectively. A vacuum layer of 15 Å was applied to avoid the interaction between adjacent periodic slabs. Moreover, the DFT-D3 method proposed by Grimme[38] was considered to correct the effect of vdW interaction. The Grimme DFT-D3 method is widely used and is thought to better describe the weak vdW interactions between the monolayer MSN and Gr than the DFT-D2 method. Instead of using a semi-empirical dispersion-correlated as in DFT-D2, the dispersion coefficients are now computed *ab initio* by time-dependent DFT employing known recursion relations for the higher-multipole terms.

3. Results and discussion

3.1. Electronic properties of the MSN and MSN/Gr heterostructure without defects

The optimized lattice constants of the MSN and Gr are 2.91 Å and 2.46 Å, respectively, which are in good agreement with other works.[39–41] As can be seen from the top views of the MSN and Gr (as shown in Fig. 1(a) and 1(c)), MSN and Gr are both composed of hexatomic rings. From the side views, the MSN is built by an N–Si–N–Mo–N–Si–N septuple-atomic layer and the Gr is built by a single-atomic layer. Figures 1(b) and 1(d) show the band structures of the monolayer MSN and Gr, and the Fermi level is set to zero. The calculated value of the band gap of the MSN is 1.80 eV, which is slightly smaller than the experimental results (1.94 eV),[30] but agrees with the results calculated by other researchers.[42] The conduction band minimum (CBM) and valence band maximum (VBM) of the MSN are located at the high-symmetry K and Γ points in the Brillouin zone, respectively. The CBM and VBM are located at different high-symmetry points in the Brillouin zone, so the MSN is an indirect band gap semiconductor. However, the calculated value of the band gap of the Gr is approximately equal to zero with the Fermi level just passing through the Dirac point. The Dirac cone of the Gr is located at the high-symmetry K point. The energy and momentum of the electrons both have a linear dispersion relationship, which makes the effective mass of Gr relativistic electrons approximately equal to zero.

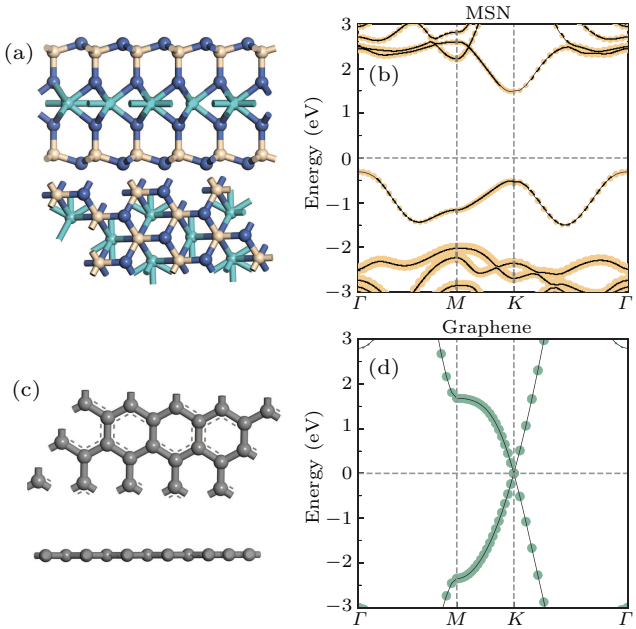


Fig. 1. The side and top views of (a) MSN and (c) Gr; band structures of (b) MSN and (d) Gr. The Fermi level is set to zero.

The cohesive energy ($E_{\rm coh}$) is firstly considered to assess the possibility of experimentally synthesizing the MSN

$$E_{\rm coh}=\frac{E_{\rm tot}-nE_{\rm Mo}-2nE_{\rm Si}-4nE_{\rm N}}{7n}, \tag{1}$$

where $E_{\rm tot}$, $E_{\rm Mo}$, $E_{\rm Si}$ and $E_{\rm N}$ are the energy of the MSN supercell and the ground state total energy of a single Mo, Si and N atom, respectively. The n represents the cell expansion multiplier of the MSN supercell. In our calculation, the value of n is equal to 1. The calculated cohesive energy is −8.44 eV/atom, indicating the possibility of experimentally synthesizing the MSN structure.

The pristine MSN/Gr heterostructure is prepared using a $\sqrt{3}\times\sqrt{3}\times1$ MSN supercell and a $2\times2\times1$ Gr supercell with a considerable lattice mismatch of 2.39%. The side and top views of the MSN/Gr heterostructure are shown in Fig. 2(a).

After the structural relaxation, the equilibrium interface distance, which is defined as the distance from the Gr layer to the lowermost Si layer of the MSN, is 3.35 Å. As shown in Fig. 2(b), the band structure of the MSN/Gr heterostructure is a simple superposition of the MSN band structure and the Gr band structure. The yellow and green lines represent the contributions of the MSN and Gr, respectively. However, due to the band folding of the MSN, the position of the CBM of the MSN changes from the original K point to the Γ point, while the position of the VBM of the MSN remains unchanged. The MSN achieves the transition from the original indirect bandgap semiconductor to the direct bandgap semiconductor.

Then, we plot the plane-averaged differential charge density along the Z-plane in Fig. 2(c) to investigate the charge transfer properties at the interface of the MSN/Gr heterostructure. The plane-averaged differential charge density ($\Delta\rho$) is defined as follows:

$$\Delta\rho = \rho_{\mathrm{vdW}} - \rho_{\mathrm{MSN}} - \rho_{\mathrm{Gr}}, \tag{2}$$

where ρ_{vdW}, ρ_{MSN} and ρ_{Gr} are the plane-averaged charge densities of the MSN/ Gr with or without defects, the isolated MSN single layer and the isolated Gr layer. The pink and blue areas represent the accumulation and depletion of the charges, respectively. We find charge transfer behavior at the interface of the MSN/Gr heterostructure. In addition, the charges are accumulated in the MSN layer and depleted in the Gr layer, implying that the charges are transferred from the Gr layer to the MSN layer. Due to the charge transfer behavior at the interface, a built-in electric field is generated at the interface pointing from the Gr layer to the MSN layer.

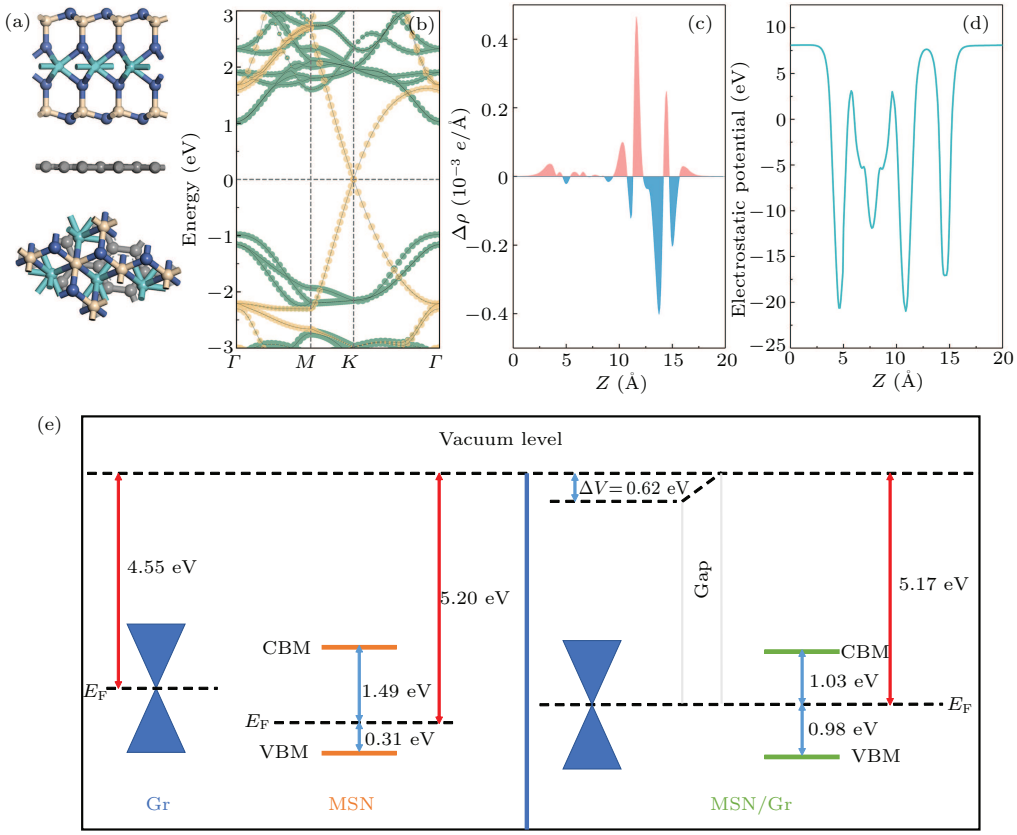


Fig. 2. (a) The side and top views of the MSN/Gr heterostructure. (b) The projected band structure of the MSN/Gr heterostructure. The Fermi level is set to zero and the yellow and green lines represent the contributions of the MSN and Gr, respectively. (c) The plane-averaged differential charge density between two interfaces along the Z-plane of the MSN/Gr heterostructure. The pink and blue areas represent the accumulation and depletion of the charges, respectively. (d) The effective electrostatic potential of the MSN/Gr heterostructure. (e) The band alignments of the Gr and MSN before (left) and after (right) formation of the heterostructure. E_{F} is the Fermi energy level.

Figure 2(d) shows the effective electrostatic potential of the MSN/Gr heterostructure. When the MSN/Gr heterostructure is completely relaxed, the effective electrostatic potential of the MSN layer is deeper than that of the Gr layer, indicating the existence of a strong electrostatic field between the two layers. The effective electrostatic potential in the MSN layer part shows a symmetrical property due to the symmetry of the MSN structure. The significant potential drop between the MSN and Gr leads to the generation of a built-in electric field at the interface of the MSN/Gr heterostructure. The band alignments of the Gr and MSN before and after the formation of the heterostructure are depicted in Fig. 2(e). We calculate the work function W_{M} of the MSN and Gr, which can be defined as the difference between the vacuum energy level and the Fermi energy level

$$W_{\mathrm{M}} = E_{\mathrm{vacuum}} - E_{\mathrm{F}}, \tag{3}$$

where E_{vacuum} and E_{F} are the energy of the vacuum energy level and the Fermi energy level, respectively. The calculated work function W_{M} of the MSN is 5.20 eV, which is greater than 4.55 eV of the Gr, as shown in Fig. 2(e). The charge transfer from the layer with a small work function (Gr) to the layer with a large work function (MSN) is attributed to the disparity in the work functions between these two layers. As the amount of charge transfer increases, the Fermi energy levels of the Gr and MSN keep decreasing and increasing, respectively, and eventually both reach the same energy level. It is worth noting that the work function of the MSN/Gr heterostructure (5.17 eV) lies just between the work functions of the Gr and MSN, implying that charges are accumulated in the MSN layer and depleted in the Gr layer. This is also consistent with previous conclusions on the plane-averaged differential charge density.

3.2. Electronic properties of the MSN and MSN/Gr heterostructure with defects

Before studying the heterostructure with defects, first, we study four monolayer MSN with defects, namely MSN_$V_{\text{N-in}}$, MSN_$V_{\text{N-out}}$, MSN_V_{Si} and MSN_V_{Mo}, respectively. In practical experiments, the defect formation energy E_{f} is a key parameter that can directly reflect the difficulty of the formation of the vacancy defects and the stability of the defective structures. It is very necessary to explore the formation energy E_{f} of the defective structures, which can be defined by the following equation:

$$E_{\text{f}} = E_{\text{vacancy}} - E_{\text{intrinsic}} + m\mu_X, \tag{4}$$

where E_{vacancy} and $E_{\text{intrinsic}}$ are the energy of the MSN (MSN/Gr) with and without defects, while m is the number of the removed X atoms and μ_X is the chemical potential of the removed X atom. The chemical potentials of the removed Si, Mo and N atoms are energy of per atom of their corresponding stable structures. For the removed Si and Mo atoms, the reference phases used are their bulk structures. For the removed N atom, the reference phase used is its stable N_2 molecule in the gas phase. The positive (negative) value of the formation energy denotes the non-spontaneous (spontaneous) process. The values of the calculated formation energy E_{f} are listed in Table 1. All obtained values of the formation energy for the four defective structures are negative, implying that the four defective structures are stable in the air. Among them, the MSN_V_{Si} model has the smallest value of the formation energy (-10.02 eV) and the MSN_$V_{\text{N-in}}$ model has the largest value of the formation energy (-3.76 eV). Our results demonstrate that the MSN_V_{Si} is the most stable model and the MSN_$V_{\text{N-in}}$ is the most unstable one.

Figures 3(a)–3(d) show the side views of the pristine MSN with vacancies and the positions of the defective atoms are circled in red. In our calculations, spin polarization was considered. The band structures of the monolayer MSN with vacancies are shown in Figs. 3(e)–4(h). It is noteworthy that when four different vacancy defects are introduced, defective energy levels are generated near the Fermi energy level in both the up and down spin channels. It can also be easily seen that the band structures of both the MSN_$V_{\text{N-out}}$ and the MSN_V_{Mo} models show perfect symmetry in both the up and down spin channels, indicating that N-out and Mo vacancies cannot introduce magnetism into the pristine MSN. However, when N-in and Si vacancies are introduced, the up and down spin channels show asymmetry, suggesting that the MSN_$V_{\text{N-in}}$ and MSN_V_{Si} models are magnetic systems with magnetic moments of 0.809 μ_{B}/cell and 1.966 μ_{B}/cell, respectively.

Table 1. Calculated equilibrium interface distance (D_{eq}), binding energy (E_{b}), formation energy (E_{f}), work function (W_{F}) and total magnetic moment (M).

	D_{eq} (Å)	E_{b} (eV)	E_{f} (eV)	W_{F} (eV)	M (μ_{B}/cell)
Gr	–	–	–	4.55	0
MSN	–	–	–	5.20	0
MSN_$V_{\text{N-in}}$	–	–	–3.76	4.60	0.809
MSN_$V_{\text{N-out}}$	–	–	–4.96	4.68	0
MSN_V_{Si}	–	–	–10.02	7.82	1.966
MSN_V_{Mo}	–	–	–7.24	5.17	0
MSN/Gr	3.35	–0.69	–	5.17	0
MSN/Gr_$V_{\text{N-in}}$	3.38	–0.43	–3.95	4.56	0.756
MSN/Gr_$V_{\text{N-out}}$	3.36	–0.42	–5.11	4.59	0
MSN/Gr_V_{Si}	3.41	–1.04	–11.13	7.68	1.828
MSN/Gr_V_{Mo}	3.38	–0.43	–7.79	5.12	0

When N-in vacancy is introduced, the Fermi energy level passes through the defective energy level in the up-spin channel. While in the down-spin channel, there is no overlap between the Fermi energy level and the energy band, so the MSN_$V_{\text{N-in}}$ model is a half-metal. In contrast, the MSN_V_{Mo} model is still a semiconductor. Unlike both the MSN_$V_{\text{N-in}}$ and MSN_V_{Mo} models, the MSN_$V_{\text{N-out}}$ and MSN_V_{Si} models exhibit metallicity. Furthermore, the work functions of four defective monolayers are also calculated in our work. Our calculation shows that the work function of the pristine MSN decreases when N and Mo vacancies are introduced and increases when Si vacancy is introduced.

We then use four defective monolayers to match Gr to form MSN/Gr heterostructure with vacancies, namely, MSN/Gr_$V_{\text{N-in}}$, MSN/Gr_$V_{\text{N-out}}$, MSN/Gr_V_{Si} and MSN/Gr_V_{Mo}, respectively. As listed in Table 1, the obtained equilibrium interface distances of the four defective heterostructures are 3.38 Å, 3.36 Å, 3.41 Å and 3.38 Å, respectively, which are quite close to the distance of the pristine MSN/Gr heterostructure and are all larger than the pristine MSN/Gr heterostructure.

The binding energy (E_b) can be used to describe the stability of the MSN/Gr heterostructure with and without defects

$$E_b = E_{vdW} - E_{Gr} - E_{MSN}, \tag{5}$$

where E_{vdW}, E_{Gr} and E_{MSN} are the energy of the MSN/Gr heterostructure with and without defects, the energy of the isolated Gr and MSN, respectively. A smaller value of the binding energy E_b indicates a more stable heterostructure. For the pristine MSN/Gr heterostructure, the calculated binding energy E_b is -0.69 eV, indicating that the pristine MSN/Gr heterostructure is a stable structure. The values of the binding energy of the MSN/Gr_V_{N-in}, MSN/Gr_V_{N-out} and MSN/Gr_V_{Mo} models are extremely close to each other and are all greater than the pristine MSN/Gr heterostructure. While the value of the binding energy of the MSN/Gr_ V_{Si} model is smaller than the pristine MSN/Gr heterostructure, which means that the MSN/Gr_V_{Si} model is more stable than the pristine MSN/Gr heterostructure. Furthermore, the values of the formation energy E_f of four defective heterostructures are all negative, indicating that all models are stable. Like the monolayer MSN with vacancies, the model for Si vacancy defect is the most stable model and the N-in vacancy defect is the most unstable one. The work function of the pristine MSN/Gr decreases when N and Mo vacancies are introduced and increases when Si vacancy is introduced.

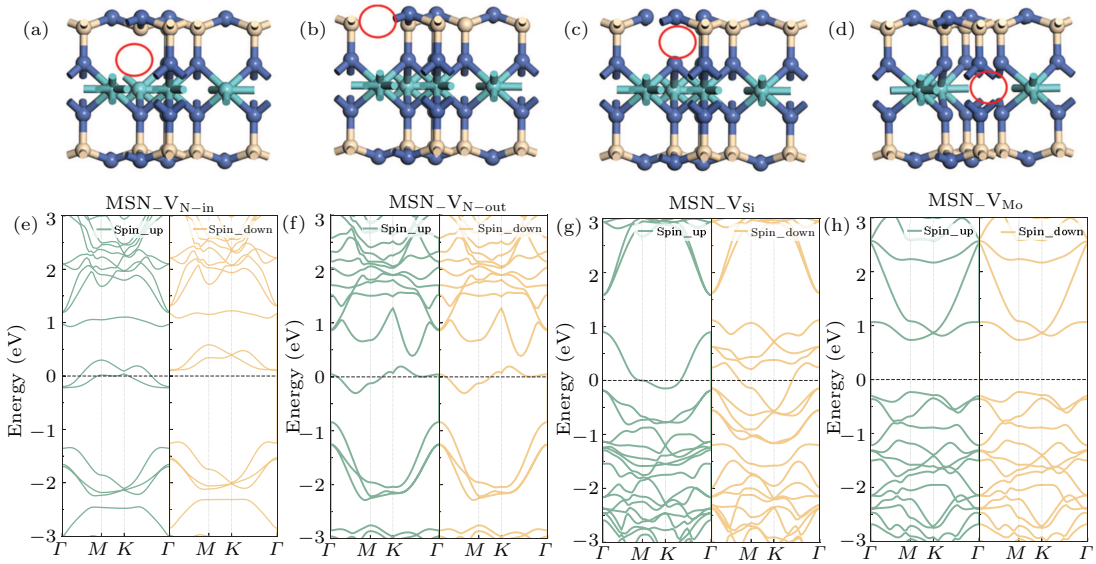


Fig. 3. The side views of the intrinsic MSN with vacancies: (a) MSN_V_{N-in}, (b) MSN_V_{N-out}, (c) MSN_V_{Si} and (d) MSN_V_{Mo}. Band structures of the monolayer MSN with vacancies: (e) MSN_V_{N-in}, (f) MSN_V_{N-out}, (g) MSN_V_{Si} and (h) MSN_V_{Mo}. Fermi level is set to zero.

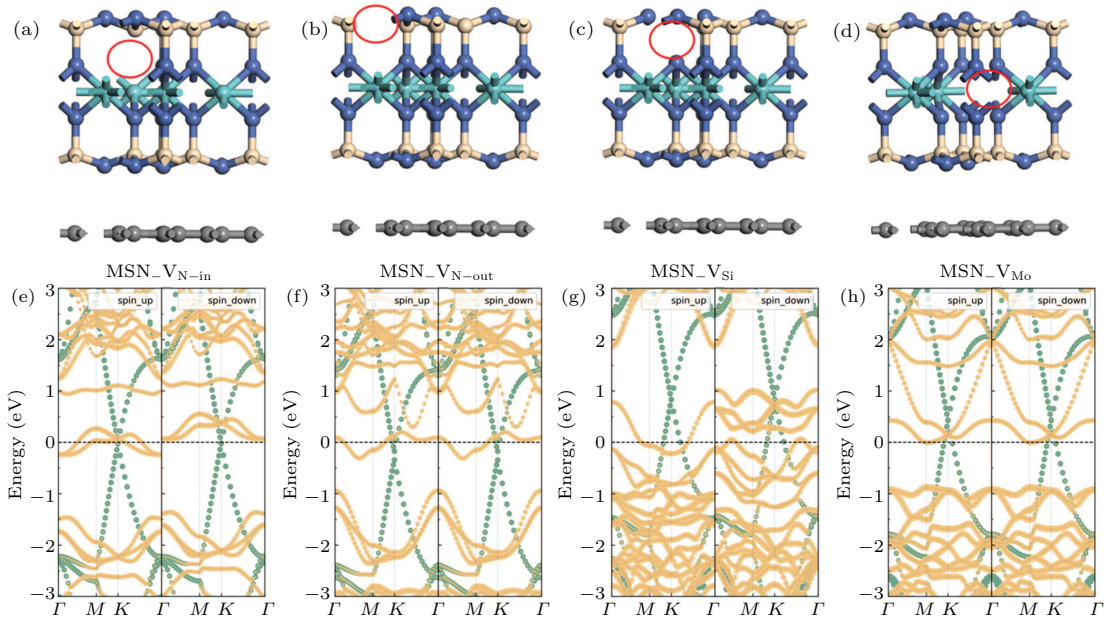


Fig. 4. The side views of the MSN/Gr heterostructure with vacancies: (a) MSN/Gr_V_{N-in}, (b) MSN/Gr_V_{N-out}, (c) MSN/Gr_V_{Si} and (d) MSN/Gr_V_{Mo}. The projected band structures of the MSN/Gr heterostructure with vacancies: (e) MSN/Gr_V_{N-in}, (f) MSN/Gr_V_{N-out}, (g) MSN/Gr_V_{Si} and (h) MSN/Gr_V_{Mo}. The Fermi level is set to zero and the yellow and green lines represent the contributions of MSN and Gr, respectively.

Figures 4(a)–4(d) show the side views of the MSN/Gr heterostructure with vacancies and the positions of the defective atoms are circled in red. Figures 4(e)–4(h) correspond to the projected band structures after the introduction of N-in, N-out, Si and Mo vacancy defects, respectively. Just like the monolayer MSN with vacancies, the up and down spin channels of N-out and Mo vacancy defects are symmetrical and neither system is magnetic. In contrast, the up and down spin channels of N-in and Si vacancy defects are asymmetrical and both are magnetic systems with magnetic moments of 0.756 μ_B/cell and 1.828 μ_B/cell, respectively. We also find that the band structure of the defective heterostructure is just a simple superposition of its corresponding defective monolayer MSN and Gr band structures.

Furthermore, in order to investigate the specific origin of magnetism, the magnetic moments contributed by the atomic orbitals of C, N, Si, Mo atoms of four magnetic models (MSN_V_{N-in}, MSN_V_{Si}, MSN/Gr_V_{N-in} and MSN/Gr_V_{Si}) are listed in Table 2. For the MSN_V_{N-in} model, the magnetic moments contributed by 2s and 2p atomic orbitals of N atoms are 0.000 μ_B/cell and 0.072 μ_B/cell, respectively. The magnetic moments contributed by 3s and 3p atomic orbitals of Si atoms are both −0.00 μ_B/cell and the magnetic moments contributed by 4p, 4d and 5s atomic orbitals of Mo atoms are 0.020 μ_B/cell, 0.711 μ_B/cell and 0.008 μ_B/cell, respectively. The total magnetic moment of the MSN_V_{N-in} model is 0.809 μ_B/cell, which is mainly contributed by the 2p atomic orbitals of N atoms and the 4d atomic orbitals of Mo atoms. For the MSN_V_{Si} model, the total magnetic moment is 1.966 μ_B/cell and it is mainly contributed by the 2s and 2p atomic orbitals of N atoms. For the MSN/Gr_V_{N-in} and MSN/Gr_V_{Si} models, the total magnetic moments are 0.756 μ_B/cell and 1.828 μ_B/cell, respectively. The magnetic moments of the MSN/Gr_V_{N-in} and MSN/Gr_V_{Si} models contributed by atomic orbitals of C atoms are both zero, indicating that vacancies do not affect the magnetic properties of the underlying Gr but only the upper MSN. Like the MSN_V_{N-in} model, for the MSN/Gr_V_{N-in} model, the 2p atomic orbitals of N atoms and the 4d atomic orbitals of Mo atoms are the main cause of the magnetism. Like the MSN_V_{Si} model, for the MSN/Gr_V_{Si} model, the magnetic moment is mainly contributed by the 2s and 2p atomic orbitals of N atoms.

Table 2. Magnetic moments contributed by atomic orbitals of C, N, Si and Mo atoms and total magnetic moment (M).

Magnetic moments contributed by atomic orbitals	MSN_V_{N-in} (μ_B/cell)	MSN_V_{Si} (μ_B/cell)	MSN/Gr_V_{N-in} (μ_B/cell)	MSN/Gr_V_{Si} (μ_B/cell)
2s of C	–	–	0.000	0.000
2p of C	–	–	0.000	0.000
2s of N	0.000	0.086	–0.001	0.079
2p of N	0.072	1.813	0.079	1.717
3s of Si	–0.001	–0.004	0.000	–0.008
3p of Si	–0.001	–0.007	0.000	–0.008
4p of Mo	0.020	0.009	0.019	0.009
4d of Mo	0.711	0.066	0.652	0.037
5s of Mo	0.008	0.003	0.007	0.002
M	0.809	1.966	0.756	1.828

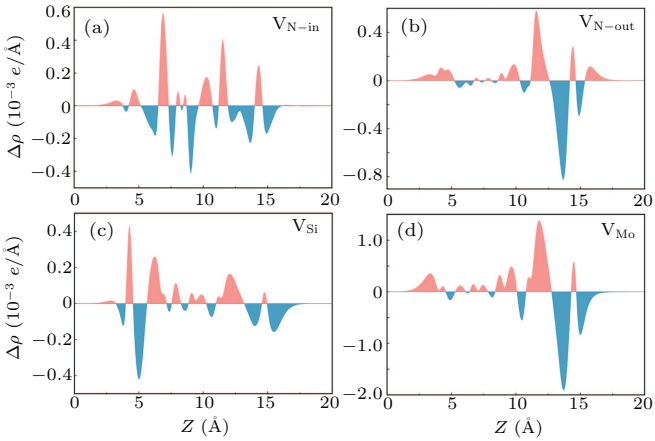


Fig. 5. The plane-averaged differential charge densities between two interfaces along the Z-plane of the MSN/Gr heterostructure with vacancies: (a) MSN/Gr_V_{N-in}, (b) MSN/Gr_V_{N-out}, (c) MSN/Gr_V_{Si} and (d) MSN/Gr_V_{Mo}. The pink and blue areas represent the accumulation and depletion of the charge, respectively.

We then plot the plane-averaged differential charge densities to investigate the charge transfer difference between the pristine and defective MSN/Gr heterostructures in Figs. 5(a)–5(d). After comparison, it is clear that charge transfer at the interface decreases after the introduction of N-in and Si vacancy defects and increases after the introduction of N-out and Mo vacancy defects. However, the charges at the interface are still depleted at the Gr layer and accumulated at the MSN layer. The direction of the built-in electric field does not change with the generation of vacancies. Obviously, N-out and Mo vacancy defects have little effect on charge transfer at the non-interfaces. While N-in and Si vacancy defects have a large effect on the charge transfer near the positions of the corresponding defective atoms.

Figures 6(a)–6(d) show the effective electrostatic potentials of the MSN/Gr heterostructure with vacancies, respectively. The introduction of Si vacancy defect creates an energy difference ($\Delta\Phi_1$) of 3.46 eV in the vacuum region between the

two sides, while the remaining three defects do not create an energy difference in the vacuum region. Four vacancy defects break the symmetry of the MSN layer part. In particular, N-out, Si and Mo vacancy defects lift the potentials at the positions of the corresponding defective atoms by 2.47 eV ($\Delta\Phi_2$), 10.28 eV ($\Delta\Phi_3$) and 6.21 eV ($\Delta\Phi_4$), respectively.

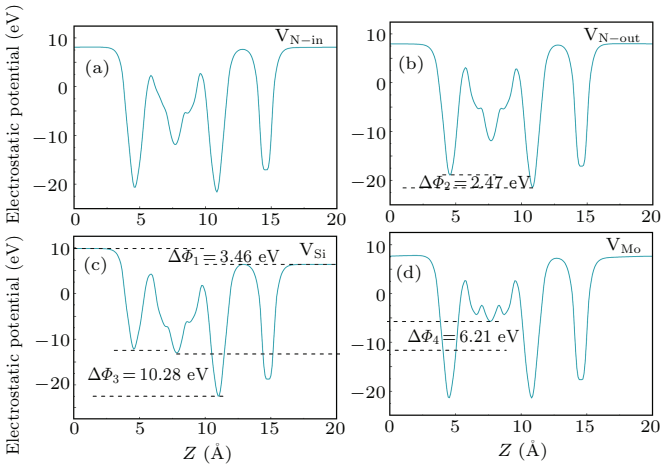


Fig. 6. The effective electrostatic potentials of the MSN/Gr heterostructure with vacancies: (a) MSN/Gr_V_{N-in}, (b) MSN/Gr_V_{N-out}, (c) MSN/Gr_V_{Si} and (d) MSN/Gr_V_{Mo}.

3.3. Modulation of the Schottky barrier height

The Schottky barrier height can commonly be effectively tuned by in-plane axial strain, external electric field and vertical strain engineering. The n-type and p-type Schottky barrier heights are defined as follows:

$$\Phi_{Bn} = E_{CBM} - E_F, \qquad \Phi_{Bp} = E_F - E_{VBM}, \tag{6}$$

where Φ_{Bn} and Φ_{Bp} represent the barrier height for electrons and holes, respectively. E_{CBM} and E_{VBM} denote the energy of the CBM and VBM of MSN. E_F is the Fermi energy level, which is set to zero in this work. When the value of Φ_{Bn} is smaller than the value of Φ_{Bp}, an n-type Schottky contact is formed at the interface of the MSN/Gr heterostructure, and vice versa for a p-type Schottky contact. According to Fig. 2(b), the calculated Φ_{Bn} and Φ_{Bp} are 1.03 eV and 0.98 eV, respectively, and the sum of Φ_{Bn} and Φ_{Bp} is equal to 2.01 eV. The value of Φ_{Bn} is larger than Φ_{Bp}, indicating a p-type Schottky is formed at the interface of the MSN/Gr heterostructure.

Since MSN/Gr heterostructure has a sizable Schottky barrier height, it is of great significance to achieve a low Schottky barrier height and contact resistance to enhance the device performance. Experimentally, one can achieve the modulation of the applied electric field by introducing pulsed ac fields or gate voltage.[43,44] The Gr and MoS_2-based electrical devices have been successfully fabricated based on this technology.[45,46] Here, we define the positive direction of the applied external electric field pointing from the Gr layer to the MSN layer, which is consistent with the direction of the built-in electric field. Figure 7 shows the projected band structures of the MSN/Gr heterostructure under different external electric fields. Compared to the original MSN/Gr heterostructure without an external electric field, we find that the electric field only shifts the band structure up and down, while the trend of the band remains largely unchanged. It is noted that the Fermi energy level shifts towards the VBM of the MSN under the positive external electric field. Conversely, the Fermi energy level shifts towards the CBM of the MSN under the negative external electric field. The MSN in the MSN/Gr heterostructure retains the same characteristics as the direct bandgap semiconductor in the original heterostructure regardless of the positive or negative applied external electric field.

Furthermore, we plot the variation of the Schottky barrier heights under different external electric fields (E_{ext}) of the MSN/Gr heterostructure in Fig. 8. It is found that when the positive external electric field is applied, the value of Φ_{Bn} gradually increases while the value of Φ_{Bp} gradually decreases. At the interface of the MSN/Gr heterostructure, the original p-type Schottky contact is maintained. When the negative external electric field is applied, the trends of Φ_{Bn} and Φ_{Bp} are opposite to those of the positive applied electric field. As the negative electric field increases, the value of Φ_{Bn} becomes smaller than the value of Φ_{Bp}, indicating that the n-type Schottky contact is formed at the interface of the MSN/Gr heterostructure. It is worth noting that the sum of Φ_{Bn} and Φ_{Bp} is almost unchanged and the variation curve is almost a straight line. We also find that when the applied electric field is large to a certain extent ($\pm$0.5 V/Å), the Schottky barrier height becomes very small (close to zero). A vanishingly small Schottky barrier height and dynamic switching between n-type and p-type Schottky contacts are of great significance for achieving energy-efficient and high-performance Schottky barrier diodes and Schottky devices.

Contact resistance originating from the Schottky barrier greatly reduces the electrical performance of Schottky devices, so we design a tunable electrical diode based on MSN/Gr vertical contacts, as shown in Fig. 9. The upward arrow indicates the positive direction of the applied electric field and the downward arrow indicates the negative direction of the applied electric field. Due to the ultra-high carrier mobility of the Gr, it can be used as an electrode to achieve efficient carrier injection. By changing the strength and direction of the external electric field, the electrical diode can be reconfigured to realize a small Schottky barrier height and dynamic switching between n-type and p-type Schottky contacts. The tunable electrical diode based on MSN/Gr vertical contacts may provide the possibility to exceed the capabilities of conventional Schottky diodes.

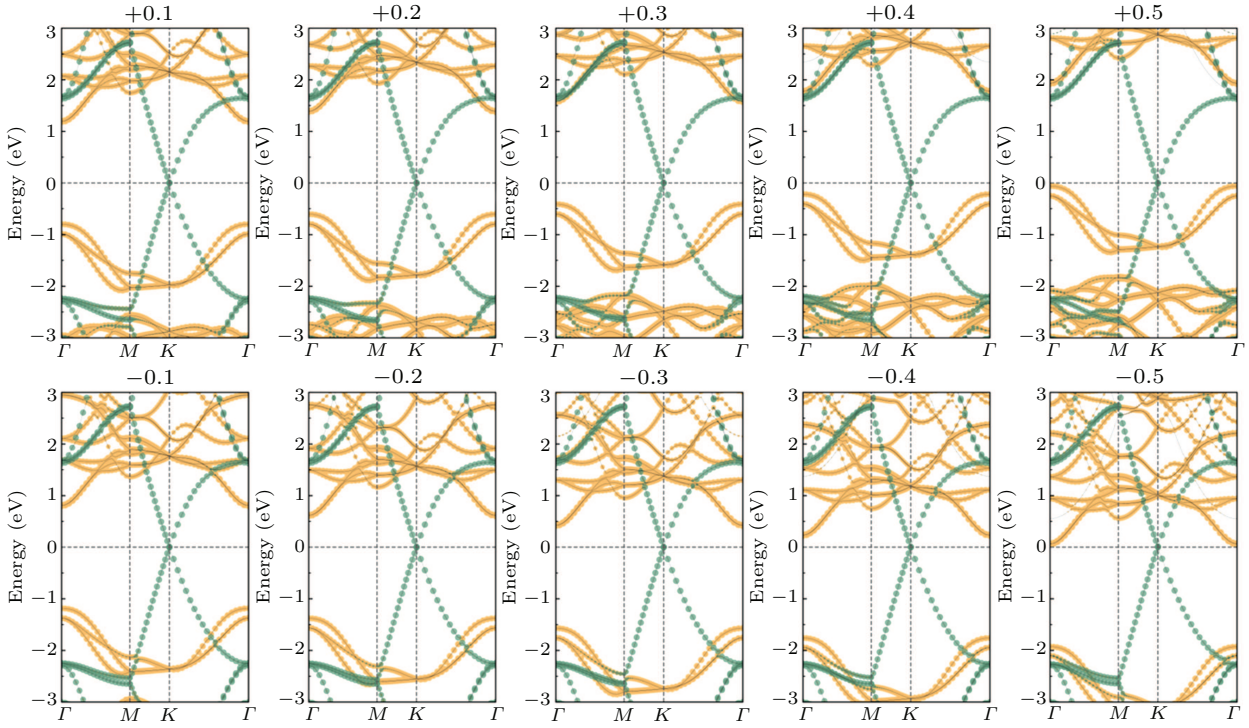


Fig. 7. The projected band structures of the MSN/Gr heterostructure under different external electric fields (ranging from −0.5 V/Å to 0.5 V/Å). The Fermi level is set to zero and the yellow and green lines represent the contributions of the MSN and Gr, respectively.

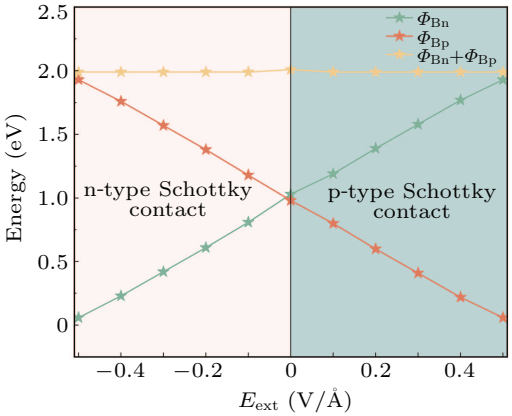


Fig. 8. The variation of the Schottky barrier heights under different external electric fields (E_{ext}) of the MSN/Gr heterostructure.

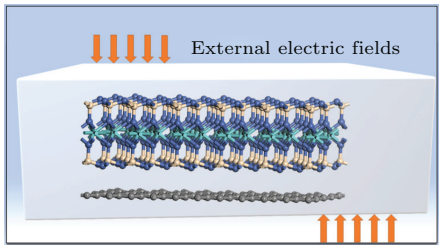


Fig. 9. Schematic diagram of a tunable electrical diode based on MSN/Gr vertical contacts.

4. Conclusion

In summary, the effects of vacancy and external electric field on the electronic properties of the MSN/Gr heterostructure have been systematically investigated in this study based on first-principles calculation. Our results show the following:

(i) The band structure of the pristine MSN/Gr heterostructure is a simple superposition of the MSN band structure and the Gr band structure. We also find a charge transfer phenomenon at the interface between the Gr layer and the MSN layer, leading to the generation of a built-in electric field pointing from the Gr layer to the MSN layer.

(ii) For the pristine monolayer MSN, the introduction of N-in vacancy defect transforms the pristine MSN from a semiconductor to a half-metal. The introduction of N-out and Si vacancy defects transforms the pristine MSN from a semiconductor to a metal. While the introduction of Mo vacancy defect maintains the semiconductor nature of pristine MSN. For the pristine monolayer MSN and MSN/Gr heterostructure, the introduction of N-out and Mo vacancy defects cannot introduce magnetism into the original non-magnetic system. However, N-in and Si vacancy defects convert the original non-magnetic system into a magnetic system.

(iii) The work functions of the pristine monolayer MSN and MSN/Gr heterostructure decrease when N and Mo vacancies are introduced and increase when Si vacancy is introduced. In addition, the charge transfer at the interface of the MSN/Gr heterostructure decreases after the introduction of N-in and Si vacancy defects and increases after the introduction of N-out and Mo vacancy defects. N-out, Si and Mo vacancy defects raise the potentials at the positions of the corresponding defective atoms.

(iv) External electric field is an effective method to modulate the Schottky barrier height of the MSN/Gr heterostructure. Under the positive external electric field, the p-type Schottky

contact is maintained. While under the positive external electric field, the MSN/Gr heterostructure can be modulated to realize the transition from the p-type contact to the n-type Schottky contact. Our results may provide a theoretical basis for the fabrication of energy-efficient and high-performance Schottky barrier diodes and Schottky devices.

Acknowledgements

Project supported by the Industry and Education Combination Innovation Platform of Intelligent Manufacturing and Graduate Joint Training Base at Guizhou University (Grant No. 2020-520000-83-01-324061), the National Natural Science Foundation of China (Grant No. 61264004), and the High-level Creative Talent Training Program in Guizhou Province of China (Grant No. [2015]4015).

References

[1] Sangwan V K and Hersam M C 2018 *Annu. Rev. Phys. Chem.* **69** 299
[2] Duerloo K A N, Ong M T and Reed E J 2012 *J. Phys. Chem. Lett.* **3** 2871
[3] Taft E and Philipp H 1965 *Phys. Rev.* **138** A197
[4] Zhu X, Li F, Wang Y, Qiao M and Li Y 2018 *J. Mater. Chem. C* **6** 4494
[5] Akinwande D, Brennan C J, Bunch J S, Egberts P, Felts J R, Gao H, Huang R, Kim J S, Li T and Li Y 2017 *Extreme Mech. Lett.* **13** 42
[6] Novoselov K S, Geim A K, Morozov S V, Jiang D E, Zhang Y, Dubonos S V, Grigorieva I V and Firsov A A 2004 *Science* **306** 666
[7] Li D and Kaner R B 2008 *Science* **320** 1170
[8] Liu L, Feng Y and Shen Z 2003 *Phys. Rev. B* **68** 104102
[9] Kan E, Ren H, Wu F, Li Z, Lu R, Xiao C, Deng K and Yang J 2012 *J. Phys. Chem. C* **116** 3142
[10] Neupane H K and Adhikari N P 2021 *Nepal J. Sci. Technol.* **20** 55
[11] Carvalho A, Wang M, Zhu X, Rodin A S, Su H and Castro Neto A H 2016 *Nat. Rev. Mater.* **1** 16061
[12] Liu H, Neal A T, Zhu Z, Luo Z, Xu X, Tománek D and Ye P D 2014 *ACS Nano* **8** 4033
[13] Kamal C and Ezawa M 2015 *Phys. Rev. B* **91** 085423
[14] Wang Y, Ye M, Weng M, Li J, Zhang X, Zhang H, Guo Y, Pan Y, Xiao L and Liu J 2017 *ACS Appl. Mater. Interfaces* **9** 29273
[15] Manzeli S, Ovchinnikov D, Pasquier D, Yazyev O V and Kis A 2017 *Nat. Rev. Mater.* **2** 17033
[16] Wang Q H, Kalantar-Zadeh K, Kis A, Coleman J N and Strano M S 2012 *Nat. Nanotechnol.* **7** 699
[17] Liang Q, Zhang Q, Zhao X, Liu M and Wee A T 2021 *ACS Nano* **15** 2165
[18] Liu K K, Zhang W, Lee Y H, Lin Y C, Chang M T, Su C Y, Chang C S, Li H, Shi Y and Zhang H 2012 *Nano Lett.* **12** 1538
[19] Li H, Wu J, Yin Z and Zhang H 2014 *Acc. Chem. Res.* **47** 1067
[20] Shi J, Ma D, Han G F, Zhang Y, Ji Q, Gao T, Sun J, Song X, Li C and Zhang Y 2014 *ACS Nano* **8** 10196
[21] Liu X, Wang Y, Yang Y, Lv W, Lian G, Golberg D, Wang X, Zhao X and Ding Y 2020 *Nano Energy* **70** 104550
[22] Nourbakhsh A, Zubair A, Sajjad R N, Tavakkoli KG A, Chen W, Fang S, Ling X, Kong J, Dresselhaus M S and Kaxiras E 2016 *Nano Lett.* **16** 7798
[23] Jiao Y, Hafez A M, Cao D, Mukhopadhyay A, Ma Y and Zhu H 2018 *Small* **14** 1800640
[24] Kumar R, Zheng W, Liu X, Zhang J and Kumar M 2020 *Adv. Mater. Technol.* **5** 1901062
[25] Zhang X, Zhang R, Niu S, Zheng J and Guo C 2019 *Appl. Surf. Sci.* **475** 355
[26] Huang Z, Han W, Tang H, Ren L, Chander D S, Qi X and Zhang H 2015 *2D Mater.* **2** 035011
[27] Mikhaleva N S, Visotin M A, Kuzubov A A and Popov Z I 2017 *J. Phys. Chem. C* **121** 24179
[28] Neupane H and Adhikari N 2020 *Comput. Condens. Matter* **24** e00489
[29] Neupane H K and Adhikari N P 2021 *J. Mol. Model.* **27** 1
[30] Hong Y L, Liu Z, Wang L, Zhou T, Ma W, Xu C, Feng S, Chen L, Chen M L and Sun D M 2020 *Science* **369** 670
[31] Lu S, Zhang Y, Lou F, Guo K and Yu Z 2022 *Appl. Surf. Sci.* **579** 152234
[32] Nguyen C V, Nguyen C Q, Nguyen S T, Ang Y S and Hieu N V 2022 *J. Phys. Chem. Lett.* **13** 2576
[33] Xiao C, Sa R, Cui Z, Gao S, Du W, Sun X, Zhang X, Li Q and Ma Z 2021 *Appl. Surf. Sci.* **563** 150388
[34] Kresse G and Hafner J 1993 *Phys. Rev. B* **47** 558
[35] Kresse G and Hafner J 1994 *Phys. Rev. B* **49** 14251
[36] Perdew J P, Burke K and Ernzerhof M 1996 *Phys. Rev. Lett.* **77** 3865
[37] Blöchl P E 1994 *Phys. Rev. B* **50** 17953
[38] Grimme S, Antony J, Ehrlich S and Krieg H 2010 *J. Chem. Phys.* **132**
[39] Yang C, Song Z, Sun X and Lu J 2021 *Phys. Rev. B* **103** 035308
[40] Wu Q, Cao L, Ang Y S and Ang L K 2021 *Appl. Phys. Lett.* **118**
[41] Nie S, Bartelt N C, Wofford J M, Dubon O D, McCarty K F and Thürmer K 2012 *Phys. Rev. B* **85** 205406
[42] Mortazavi B, Javvaji B, Shojaei F, Rabczuk T, Shapeev A V and Zhuang X 2021 *Nano Energy* **82** 105716
[43] Kwon J, Lee J Y, Yu Y J, Lee C H, Cui X, Hone J and Lee G H 2017 *Nanoscale* **9** 6151
[44] Vicario C, Monoszlai B and Hauri C P 2014 *Phys. Rev. Lett.* **112** 213901
[45] Bokdam M, Khomyakov P A, Brocks G, Zhong Z and Kelly P J 2011 *Nano Lett.* **11** 4631
[46] Sachs B, Britnell L, Wehling T, Eckmann A, Jalil R, Belle B, Lichtenstein A, Katsnelson M, Novoselov K 2013 *Appl. Phys. Lett.* **103** 25